From Allylic Alcohols to Aldols by Using Iron Carbonyls as Catalysts: Computational Study on a Novel Tandem Isomerization–Aldolization Reaction

Vicenç Branchadell,*[a] Christophe Crévisy,[b] and René Grée*[b, c]

Abstract: The tandem isomerization–aldolization reaction between allyl alcohol and formaldehyde mediated by $[Fe(CO)_3]$ was studied with the density functional B3LYP method. Starting from the key $[(enol)Fe(CO)_3]$ complex, several reaction paths for the reaction with formaldehyde were explored. The results show that the most favorable reaction path involves first an enol/allyl alcohol ligand-exchange process followed by direct condensation of formaldehyde with the free enol. During this process, formation of the new C–C bond takes place simultaneously with a proton transfer between the enol and the aldehyde. Therefore, the role of $[Fe(CO)_3]$ is to catalyze the allyl alcohol to enol isomerization affording the free enol, which adds to the aldehyde in a carbonyl-ene type reaction. Similar results were obtained for the reaction between allyl alcohol and acetaldehyde.

Keywords: aldol reaction · density functional calculations · ene reaction · enols · iron

Introduction

Transition-metal-mediated isomerization of allylic alcohols such as **1** to enols **2** and to saturated carbonyls **3** is a known reaction.[1,2] Various types of organometallic complexes can perform this transformation, but among them iron carbonyls proved to have both a good efficiency and a broad substrate specificity.[3] When this isomerization was performed in the presence of an aldehyde a novel reaction occurred affording aldol-type derivatives **4** (Scheme 1). These compounds were obtained together with small amounts of the isomerized ketone **3** and the regioisomeric aldols **4′** (when $R = CH_2R''$).[4] From a synthetic point of view this new tandem isomerization/aldolization reaction starting from allylic alcohols appears particularly attractive, since it is a rare example of an aldol-type reaction with full atom economy which also occurs under mild and neutral conditions.[5,6] Thus, it could be a complementary approach to the elegant direct catalytic asymmetric aldol reaction that was developed recently.[7] This new tandem reaction was first performed with $[Fe(CO)_5]$ (2–5 mol %) as catalyst under irradiation conditions.[4] More recently, it was established that [(bda)Fe$(CO)_3$] (bda = *trans*-benylideneacetone) and $[(cot)Fe(CO)_3]$ (cot = cyclooctatetraene) offer a significant improvement in chemical reactivity, especially towards bulky aldehydes.

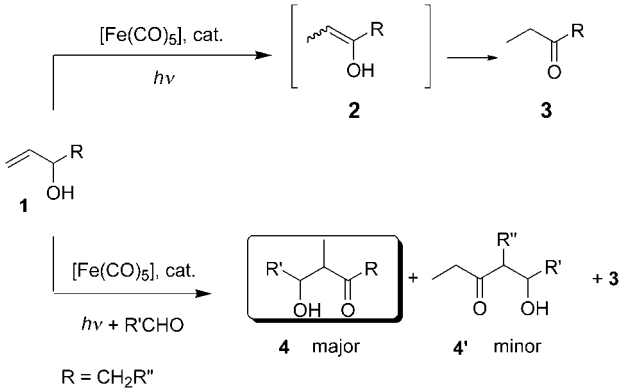

Scheme 1.

[a] Dr. V. Branchadell
Departament de Química
Universitat Autònoma de Barcelona
Edifici Cn, 08193 Bellaterra (Spain)
Fax: (+34) 935-812-920
E-mail: vicenc.branchadell@uab.es

[b] Dr. C. Crévisy, Dr. R. Grée
ENSCR, Laboratoire de Synthèses et Activations de Biomolécules, CNRS UMR 6052
Avenue du Général Leclerc, 35700 Rennes Beaulieu (France)

[c] Dr. R. Grée
New address: Université de Rennes1
Laboratoire de Synthèse et Electrosynthèse Organiques, CNRS UMR 6510
Avenue du Général Leclerc, 35042 Rennes cedex (France)
Fax: (+33) 223-236-955
E-mail: rene.gree@univ-rennes1.fr

Supporting information (Cartesian coordinates, total energies, and Gibbs energies of all structures reported in this paper) for this article is available on the WWW under http://www.chemeurj.org/ or from the author.

 DOI: 10.1002/chem.200400466

However, these catalysts led to similar regio- and stereoselectivities.[8]

This reaction could be extended to some other transition metal complexes: in the case of Rh and Ru complexes, complete regioselectivity was obtained for the aldolization,[9] and furthermore this type of reaction could also be performed in water and protic solvents[10a–b] or in ionic liquids.[10c] Finally, it was recently established that some nickel hydride complexes are also highly efficient catalysts for this reaction.[11]

From a mechanistic point of view, this new C–C bond formation raises many intriguing questions. The mechanism which is generally accepted for the isomerization of allylic alcohols mediated by iron carbonyls involves a 1,3 intramolecular hydrogen shift that occurs via η^2 complex **5**, π-allyl hydride intermediate **6**, and π-enol complex **7** (Scheme 2).[1,2]

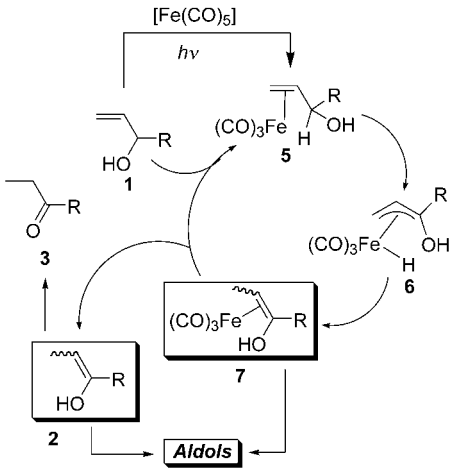

Scheme 2.

We recently reported a theoretical study on this reaction which confirmed this mechanistic proposal.[12] Based on these results it can be anticipated that both the iron carbonyl complexes **7** and free enol **2** are good candidates as reactive intermediates for addition to aldehydes affording aldol products. Therefore, as a key step towards the development of this novel reaction, it appeared important to obtain information on the possible mechanisms and the catalytic cycle. Thus, we performed an extensive computational study on different possible pathways for aldol formation. We used formaldehyde and acetaldehyde as models of the carbonyl compound, and 2-propen-1-ol as the model of allyl alcohol.

Computational Methods

All geometries were fully optimized with the B3LYP[13] density functional method implemented in Gaussian 98.[14] Energy minima and transition states were optimized by means of the standard Schlegel algorithm using redundant internal coordinates.[15] Harmonic vibrational frequencies were calculated for all structures to characterize them as energy minima (all frequencies are real) or transition states (only one imaginary frequency). In specific cases where examination of this imaginary frequency did not allow the assignment of the transition state to the corresponding reactants and products, the intrinsic reaction coordinate (IRC) was calculated.[16] In the geometry optimization we used the LANL2DZ basis set.[17] This is a double-ζ basis set for C, O, and H and for the valence space of Fe, whereas the inner shells of Fe (up to 2p) are represented by an effective core potential. This basis set was supplemented with a set of d polarization functions for C and O with exponents of 0.75 and 0.85, respectively. Electron charge distribution was analyzed with the natural population analysis of Weinhold et al.[18] Effect of solvation by cyclohexane was included for the most significant stationary points by using the conductor-like screening model.[19]

Energies of all stationary points were recalculated by single-point calculations using the 6-311+G(d,p)[20] basis set. For Fe it involves a triple-ζ basis set with a set of f polarization functions. The reported values for Gibbs energies at 1 atm and 298.15 K were obtained from energies calculated with the 6-311+G(d,p) basis sets and vibrational frequencies calculated with the LANL2DZ basis set. In several cases, the transition states were relocated, and the vibrational frequencies were calculated at the B3LYP/6-311+G(d,p) level of theory. For the reaction between free enol and formaldehyde we also performed single-point calculations using the BB1K density functional method developed by Zhao et al.[21] and based on Becke's exchange functional[22] and B95 correlation functional.[23] These calculations were performed with Gaussian 03.[24] Finally, the reaction between free enol and formaldehyde was studied by the CCSD(T) method[25] with the 6-311+G(d,p) basis set.

Results and Discussion

We considered three possible mechanisms for aldol formation (Scheme 3). Mechanism A involves first the coordination of formaldehyde to the iron atom of [(enol)$Fe(CO)_3$]

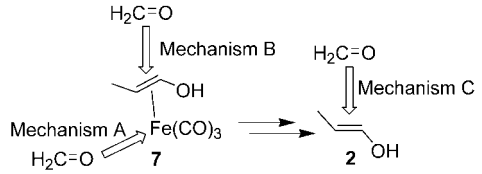

Scheme 3. Three possible mechanisms.

complex **7**, and the formation of the key C–C bond for the aldolization process occurs at a later stage. Mechanism B involves direct attack of formaldehyde on the coordinated enol of [(enol)$Fe(CO)_3$] complex **7**. Finally, in mechanism C formaldehyde reacts with free enol **2** after enol decoordination from **7**.

Mechanism A: coordination of formaldehyde to iron before formation of the key C–C bond: In the most stable structure of (enol)$Fe(CO)_3$ complex **7** the enol ligand is coordinated through the C=C bond and through one of the oxygen lone pairs (**7a** in Figure 1).[12] Decoordination of the C=C bond can lead to intermediate **7b**, in which the enol is σ-bonded to the $Fe(CO)_3$ moiety. This process has a Gibbs activation energy of 11.3 kcal mol^{-1} and a Gibbs reaction energy of 7.4 kcal mol^{-1}. Our previous computational study on the transformation of **1** into **2** established that the **7a**→**7b** rearrangement was involved in the most favorable reaction path for the enol decoordination step.[12] For this reason, we first studied the reaction path which starts with

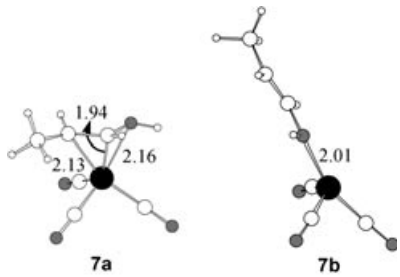

Figure 1. Structures of the [(enol)Fe(CO)$_3$] complex **7**. Selected interatomic distances in Å.

Table 1. Natural population analysis[a] for selected stationary points[b] corresponding to the reaction paths involving coordination of formaldehyde to [(enol)Fe(CO)$_3$].

	Fe(CO)$_3$	Enol	H_2CO	Aldol
8b	−0.101	0.064	0.037	
TS(8b-9a)	−0.061	0.241	−0.180	
9a	0.404			−0.404
10a	0.250			−0.250
8e	0.237	0.177	−0.414	
TS(8e-9b)	0.269	0.001	−0.270	
9b	0.334			−0.334

[a] In a.u. [b] See Figures 3 and 5.

coordination of formaldehyde to **7b**. The Gibbs energy diagram for this process is shown in Figure 2, and the structures of the most relevant stationary points are presented in Figure 3. Table 1 lists the results of natural population analyses for selected stationary points.

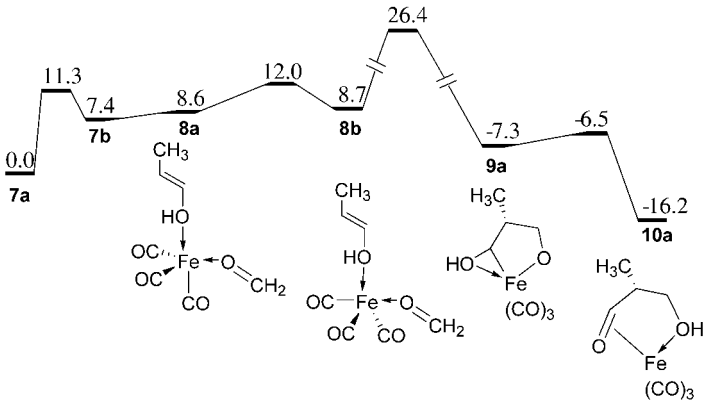

Figure 2. Gibbs energy diagram for the aldol-formation reaction involving coordination of formaldehye to **7b**. Relative Gibbs energies in kcal mol^{-1}.

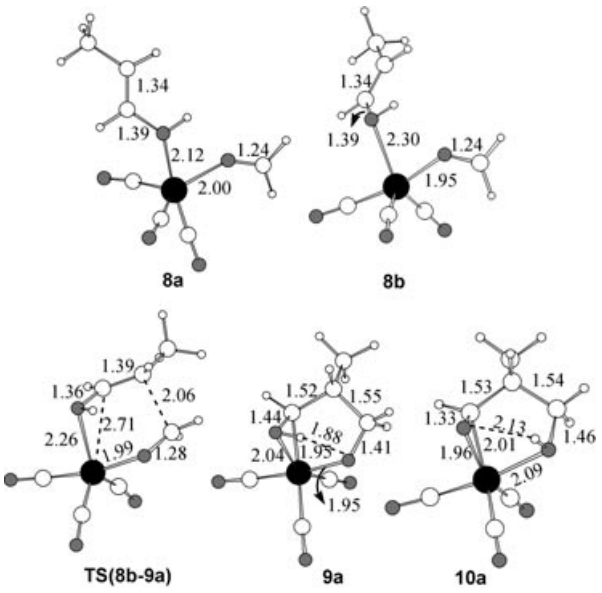

Figure 3. Structures of selected stationary points corresponding to the aldol-formation reaction starting with the coordination of formaldehyde to **7b**. Selected interatomic distances in Å.

Formaldehyde coordinates to **7b** without potential energy barrier to form **8a** with a Gibbs reaction energy of 1.2 kcal mol^{-1}. Complex **8a** is a trigonal bipyramid in which the enol group is in an axial position and the formaldehyde group is in an equatorial one. We could not find a transition state for aldol formation starting from this structure. Enol and formaldehyde ligands can easily exchange positions through a Berry pseudorotation[26] leading to **8b**. Then, rotation around the two Fe–O bonds brings the carbon atom of formaldehyde close to the C(2) atom of the enol ligand to allow formation of a new C–C bond.

This process affords the first aldol-type intermediate **9a**. The Gibbs activation energy for **8b**→**9a** is 17.7 kcal mol^{-1}, and the Gibbs reaction energy is −16 kcal mol^{-1}. The natural population analysis (see Table 1) shows that, at the transition state **TS(8b-9a)**, electron density is transferred from enol to formaldehyde, whereas the charge of the Fe(CO)$_3$ moiety only slightly changes with respect to **8b**. On the other hand, a remarkable charge transfer from the Fe(CO)$_3$ moiety to the aldol ligand is observed in **9a**. The latter compound can be formally considered as a Fe^{II} complex in which an aldol ligand is coordinated through two σ bonds (Fe–C and Fe–O) and a dative bond involving one of the OH lone pairs.

Note that intermediate **9a** is not the final aldol complex, since the hydrogen atom is still bonded to the oxygen atom of the enol. Proton transfer to the oxygen atom that originated from formaldehyde takes place with a very low Gibbs activation energy (0.8 kcal mol^{-1}) to form **10a**, which is thermodynamically more stable than **9a** ($\Delta G = -8.9$ kcal mol^{-1}). This process involves an important diminution of the charge transfer between Fe(CO)$_3$ and the aldol ligand. Complex **10a** can be viewed as a Fe^0 complex in which the aldol ligand is coordinated through the π system of the carbonyl group and one of the lone pairs of OH.

The complete reaction path from **7a** to **10a** via **8a** and **8b** has a Gibbs activation energy of 26.4 kcal mol^{-1}. Furthermore, the overall process is highly exergonic with a Gibbs reaction energy of −16.2 kcal mol^{-1}.

An alternative reaction path begins with the coordination of formaldehyde to **7a**. The Gibbs energy diagram is shown in Figure 4, and the structures of the most relevant stationary points are presented in Figure 5. The first step affords **8c**, in which the enol is coordinated only through the C=C bond. Starting from **8c** reorganization occurs in the coordination sphere of the metal to afford the intermediate **8d**, in

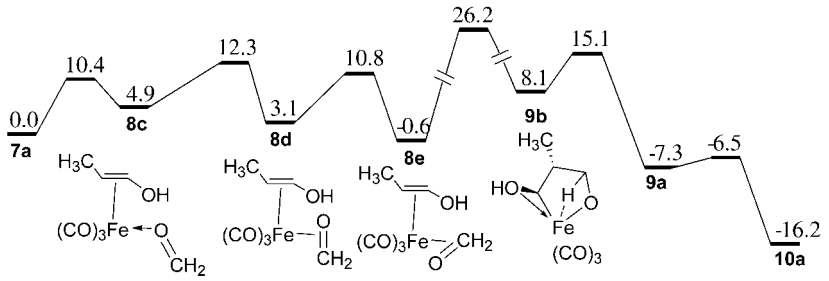

Figure 4. Gibbs energy diagram for the aldol-formation reaction involving coordination of formaldehyde to **7a**. Relative Gibbs energies in kcal mol^{-1}.

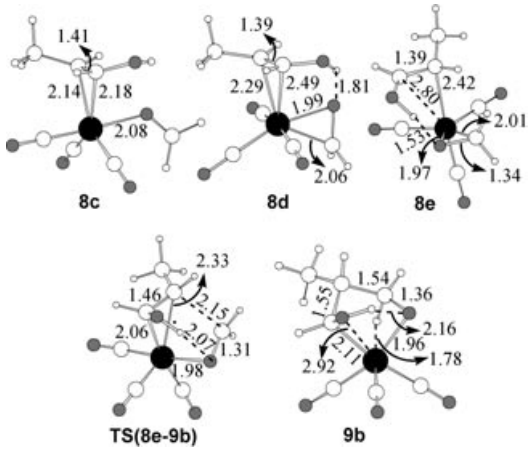

Figure 5. Structures of selected stationary points corresponding to the aldol-formation reaction starting with coordination of formaldehyde to **7a**. Selected interatomic distances in Å.

which the carbonyl group is now bonded to the iron atom in an η^2 mode and there is a hydrogen bond between the enol and carbonyl groups. Rotation around the Fe–formaldehyde bond leads to **8e**, in which the hydrogen bond between enol and formaldehyde is stronger than in **8d**. At the same time, the enol Fe–C distances notably increase. This change in the coordination mode affords a significant stabilization for **8e** as compared to **8c** ($\Delta G = -5.5$ kcal mol^{-1}).

Starting from this already preorganized complex **8e**, we localized the transition state for the key C–C bond coupling. This process affords **9b**, which is similar to **9a** (see Figure 3) but exhibits a C–H agostic interaction instead of an OH dative one. Complex **9b** can rearrange to the more stable conformer **9a** with a Gibbs activation energy of 7 kcal mol^{-1} and then to the complexed aldol **10a**. Therefore, the reaction path from **7a** to **10a** via **8c** and **8e** has a Gibbs activation energy of 26.2 kcal mol^{-1}. This represents a difference of only 0.2 kcal mol^{-1} to the path in Figure 2.

The hydrogen bond between the enol and formaldehyde ligands in **8e** is remarkably strong. Moreover, proton transfer must occur to form the final enol product. In the mechanism discussed above, this proton transfer takes place after C–C bond formation. We also considered the possibility that these two processes take place in the reverse order. Figure 6 shows the corresponding Gibbs energy diagram, and the structures of stationary points are presented in Figure 7. Proton transfer in **8e** leads to the formation of **11** with a Gibbs reaction energy of −0.04 kcal mol^{-1}. We located a transition state for this process with a very low energy barrier (0.5 kcal mol^{-1} with the LANL2DZ basis set, and 1.2 kcal mol^{-1} with 6-311+G(d,p)), but this structure becomes lower in Gibbs energy than **8e**. This result indicates

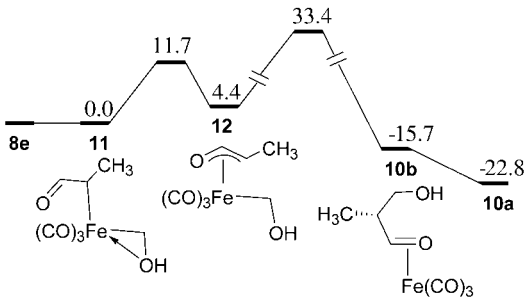

Figure 6. Gibbs energy diagram for the aldol-formation reaction involving proton transfer prior to C–C bond formation. Relative Gibbs energies in kcal mol^{-1}.

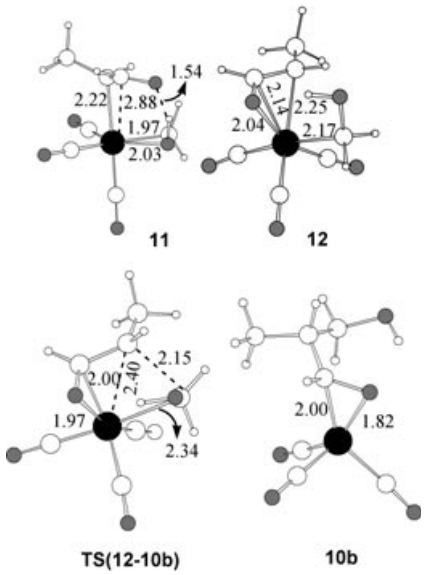

Figure 7. Structures of selected stationary points corresponding to the aldol-formation reaction involving proton transfer prior to C–C bond coupling. Interatomic distances in Å.

that the proton is mainly delocalized among both ligands. In the next step, **11** rearranges to oxoallyl complex **12**, from which a transition state for C–C bond formation was localized. This process, which can be considered as a C–C reductive elimination, leads to the formation of **10b**, in which the aldol ligand is coordinated only through the carbonyl group. Complex **10b** can then rearrange to the more stable isomer **10a**, which is 7.1 kcal mol^{-1} lower in Gibbs energy. The

Gibbs activation energy for the **12**→**10b** transformation is 29.0 kcal mol^{-1}, and 32.8 kcal mol^{-1} when calculated with respect to **7a**+formaldehyde. This value is notably larger than the 26.2 kcal mol^{-1} for the path shown in Figure 4.

Among the three reaction paths considered up to now, that involving proton transfer prior to C–C coupling (Figure 7) can be discarded. However, the two paths in which proton transfer takes place after C–C coupling (Figures 2 and 4) involve very similar Gibbs activation energies. In fact, the corresponding rate determining transition states **TS(8b-9a)** and **TS(8e-9b)** are remarkably similar. Figure 8 shows a superposition of the structures of these two transition states, which can be considered to be of the Zimmermann–Traxler type. These two structures differ mainly in the coordination of iron to the enol ligand: through oxygen in **TS(8b-9a)** and through the C=C bond in **TS(8e-9b)**. This fact has consequences for the electron distribution (see Table 1). In **TS(8b-9a)** electron density is transferred mainly from enol to formaldehyde, whereas in **TS(8e-9b)** charge transfer takes place between $Fe(CO)_3$ and formaldehyde.

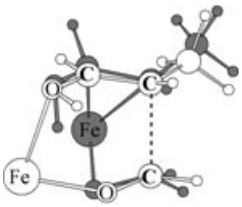

Figure 8. Superposition of the structures of transition states **TS(8b-9a)** (white) and **TS(8e-9b)** (gray) in the plane defined by the olefinic carbon atoms of the enol ligand and the carbon atom of formaldehyde. CO ligands omitted for clarity.

To complete the catalytic cycle, replacement of the aldol ligand by the allyl alcohol must be performed on the $Fe(CO)_3$ unit. We explored two different paths (Scheme 4). Starting from **10a**, decoordination of the OH group leads to the intermediate **10b** (Figure 7), in which the carbonyl group is still bonded in a η^2 mode to the $Fe(CO)_3$ unit. Then modification of the coordination mode leads to σ complex **10c** (Figure 9). Allyl alcohol can coordinate to this intermediate without potential energy barrier to give **13a**. Aldol elimination from **13a** restores the complexed allyl alcohol **5**. This process involves a rotation around the alcohol C(1)–C(2) bond to allow coordination of the OH group in **5** with a Gibbs activation energy of 4.9 kcal mol^{-1}.[12]

Alternatively, decoordination of the carbonyl group of the aldol ligand in **10a** can lead to **10d** (Figure 9). This process is slightly more favorable than the **10a**→**10c** rearrangement. The coordination of allyl alcohol to **10d** affords **13b**, from which the aldol ligand can be eliminated. The highest point in Gibbs energy for this aldol decoordination is **10d** (ΔG= 11.1 kcal mol^{-1} with respect to **10a**). Overall this process is slightly exergonic, with a Gibbs reaction energy of −1.4 kcal mol^{-1}. According to these results, the aldol decoordination step is kinetically much more favorable than the aldol formation step.

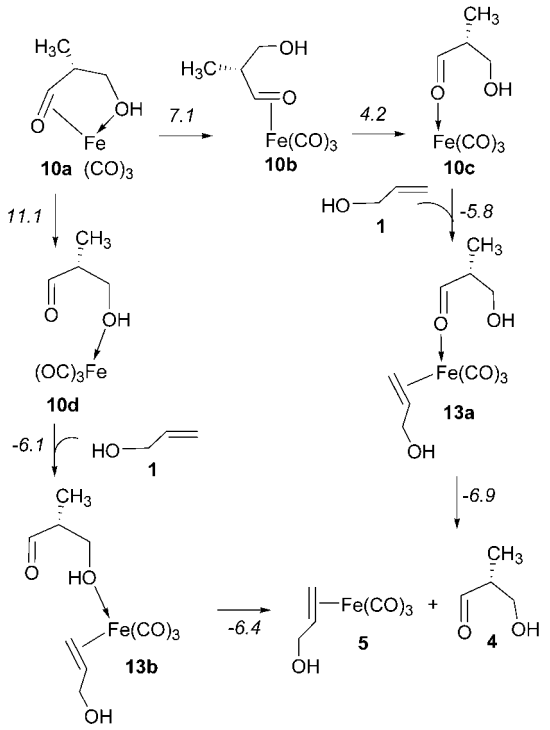

Scheme 4. ΔG values given in kcal mol^{-1}.

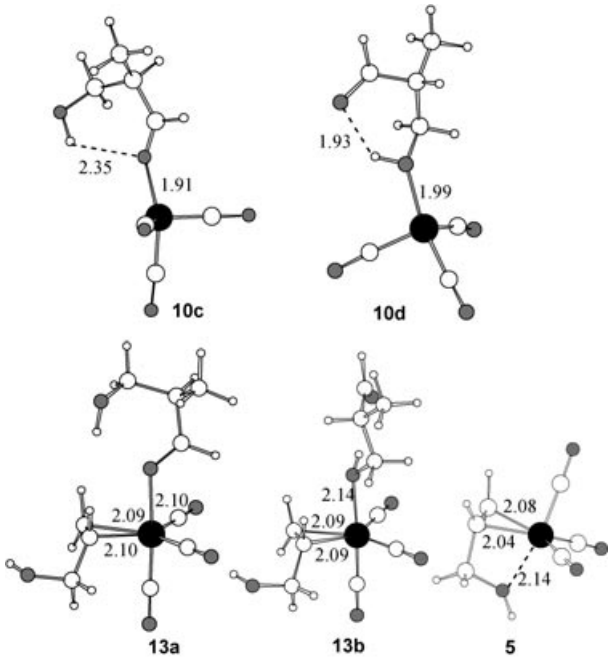

Figure 9. Structures of intermediates corresponding to the allyl alcohol/enol exchange processes shown in Scheme 4. Interatomic distances in Å.

Mechanism B: addition of formaldehyde to coordinated enol: Next we studied the direct addition of formaldehyde to the enol moiety of [(enol)$Fe(CO)_3$] complexes **7a** and **7b**.

The attack of formaldehyde from the top face and *anti* to the $Fe(CO)_3$ unit of **7a**′[27] was found to be possible, and the structure of the corresponding transition state is shown in Figure 10. This process leads to the formation of **10b**′, which

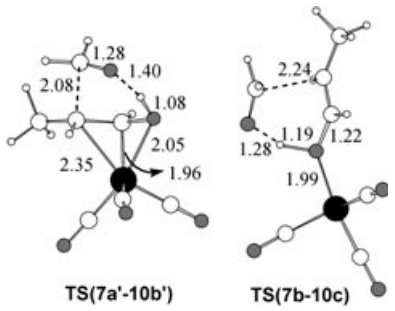

Figure 10. Structure of transition states corresponding to the attack of formaldehyde on coordinated enol. Interatomic distances in Å.

is a diasteromer of **10b**, with a Gibbs activation energy of 25.1 kcal mol^{-1} and a Gibbs reaction energy of −8.8 kcal mol^{-1}. This transition state has a hydrogen bond between the enol and the aldehyde. Examination of the transition vector shows that proton transfer from the enol ligand to the incoming formaldehyde makes an important contribution to the reaction coordinate. The natural population analysis (Table 2) shows that the electron density of the enol fragment only slightly changes on going from **7a′** to the transition state, while a remarkable charge transfer occurs from $Fe(CO)_3$ to formaldehyde. After formation of the key C–C bond, **10b′** can rearrange to the more stable isomer **10a′** (diastereomer of **10a**) with a Gibbs reaction energy of −7.8 kcal mol^{-1}. Alternatively it can also rearrange to **10c** ($\Delta G = 3.8$ kcal mol^{-1}) and coordinate an allyl alcohol molecule to complete the catalytic cycle, as described earlier (see Scheme 4).

Table 2. Natural population analysis[a] for selected stationary points[b] corresponding to the reaction paths involving direct attack of formaldehyde on [(enol)$Fe(CO)_3$].

	$Fe(CO)_3$	Enol	H_2CO
7′a	−0.042	0.042	
TS(7a′-10b′)	0.140	0.085	−0.225
7b	−0.145	0.145	
TS(7b-10c)	−0.151	0.274	−0.123

[a] In a.u. [b] See Figure 10.

We also studied the direct attack of formaldehyde on the enol moiety of **7b**, and the corresponding transition state is shown in Figure 10. This process leads to the formation of **10c** (Figure 9) with a Gibbs activation energy of 20.3 kcal mol^{-1} (25.1 kcal mol^{-1} relative to the **7a**+formaldehyde asymptote) and a Gibbs reaction energy of −12.4 kcal mol^{-1}. Complex **10c** can rearrange to the most stable isomer **10a** with $\Delta G = -11.3$ kcal mol^{-1} or coordinate an allyl alcohol molecule to complete the catalytic cycle (see Scheme 4). For this aldolization starting from **7b**, the Gibbs activation energy with respect to the **7a**+formaldehyde asymptote is 27.6 kcal mol^{-1}, 2.5 kcal mol^{-1} higher than the value corresponding to **TS(7a′-10b′)**. The natural population analysis (Table 2) shows that, on going from the reactant to the transition state, the charge transfer takes place mainly between the enol ligand and formaldehyde, whereas the charge on the $Fe(CO)_3$ fragment changes only slightly.

Mechanism C: decoordination followed by aldolization of the free enol: The last step in the **1**→**2** isomerization is decoordination of the enol. The most favorable mechanism involves the coordination of allyl alcohol to **7b** followed by enol decoordination.[12] The transition state of highest Gibbs energy is associated with the **7a**→**7b** rearrangement, so that the Gibbs activation energy for enol decordination is 11.3 kcal mol^{-1}. Moreover, the process is exergonic with a Gibbs reaction energy of −8.7 kcal mol^{-1}. The Gibbs activation energy corresponding to this decoordination is more than 10 kcal mol^{-1} lower than those corresponding to the previous aldolization processes (mechanisms A and B). Therefore, it appeared of interest to study also the attack of formaldehyde on free enol. For this carbonyl-ene type aldol reaction, we located the transition state corresponding to the formation of the aldol product **4** (Figure 11). The Gibbs activation energy associated with this process is 22.2 kcal mol^{-1}, and the Gibbs reaction energy is −9.0 kcal mol^{-1}. Examination of the transition vector shows an important contribution of proton transfer between enol and formaldehyde in the reaction coordinate, as was already been observed for **TS(7a′-10b′)** (Figure 10). In fact, there are remarkable similarities between the two transition states, the main difference being the O–H distances associated with proton transfer. The natural population analysis shows that an important charge transfer from enol to formaldehyde (0.246 a.u.) takes place at the transition state. The Gibbs activation energy calculated with respect to the **7a**+formaldehyde asymptote is 13.5 kcal mol^{-1}, a value notably lower than those associated with any of the previous reaction paths.

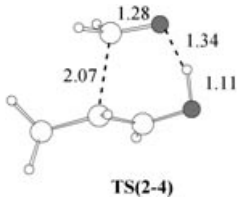

Figure 11. Structure of the transition state corresponding to the reaction between formaldehyde and 1-propen-1-ol. Interatomic distances in Å.

The potential-energy barrier associated with the reaction between **2** and formaldehyde is 9.8 kcal mol^{-1} when calculated with the 6-311+G(d,p) basis set. This value is much lower than that of 26.2 kcal mol^{-1} reported by Coitiño et al.[28] for the reaction between vinyl alcohol and formaldehyde at the Hartree–Fock level of theory. To verify that the B3LYP method provides a good description of this process, we performed single-point calculations at the BB1K/6-311+G(d,p) and CCSD(T)/6-311+G(d,p) levels, and the calculated potential energy barriers are 9.5 and 11.4 kcal mol^{-1}, respectively.

We also examined a reaction path involving attack of a free enol molecule on a species in which formaldehyde is coordinated to the $Fe(CO)_3$ moiety. One of the possible intermediates involved in mechanism A, namely, **8e** (see Figures 4 and 5), exhibits an η^2-coordinated formaldehyde and

a weak Fe–enol interaction, so that formation of a free enol seems feasible. The complete removal of the enol from **8e** to afford the [(formaldehyde)$Fe(CO)_3$] complex **14** (Figure 12) involves lowering of the Gibbs energy by

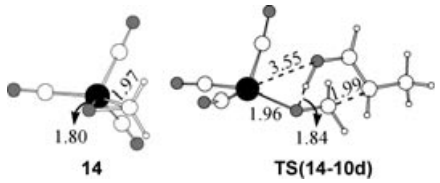

Figure 12. Structure of stationary points involved in the attack of enol **2** on [(formaldehyde)$Fe(CO)_3$] complex **14**. Interatomic distances in Å.

6.4 kcal mol^{-1}. Starting from **14**, we located the transition state for the attack of free enol from the top face of the coordinated formaldehyde and *anti* to the $Fe(CO)_3$ moiety. This process, which involves a Gibbs activation energy of 32.7 kcal mol^{-1}, leads to the formation of **10d** (see Figure 9) with $\Delta G = 1.8$ kcal mol^{-1}. The Gibbs activation energy calculated with respect to the **7a**+formaldehyde asymptote is 25.7 kcal mol^{-1}. This value is very close to those obtained in the calculations performed for mechanisms A and B, but it is much higher than for the previous reaction starting from the free enol.

Comparison of results: Table 3 lists the Gibbs energies of the rate-determining transition states associated with the reaction paths presented above. To allow comparison, they are

Table 3. Gibbs activation energies[a] for the rate-determining transition states[b] corresponding to different mechanisms of aldol formation for reactions with formaldehyde and acetaldehyde.

Mechanism	Transition state	Formaldehyde		Acetaldehyde
		gas phase	cyclohexane	gas phase
A	**TS(8b-9a)**	26.4 (26.3)	26.0	31.0
A	**TS(8e-9b)**	26.2 (26.3)	26.6	33.3
B	**TS(7a′-10b′)**	25.1 (25.1)	27.0	28.5
B	**TS(7b-10c)**	27.6 (27.6)	28.3	30.4
C	**TS(2–4)**[c]	13.5 (13.6)	12.7	19.4
C	**TS(14–10d)**	25.7 (26.1)	25.3	33.1

[a] Relative to the **7a**+aldehyde asymptote in kcal mol^{-1}. In parentheses: values calculated from B3LYP/6-311+G(d,p) geometries and frequencies. [b] See Figures 3, 5, 10, 11, and 12. [c] Relative to **7a**+aldehyde+**1**.

referred to the same origin: the **7a**+formaldehyde asymptote.

The transition state of lowest Gibbs energy is **TS(2-4)**, that is, that associated with mechanism C. The other transition states are at least 11.5 kcal mol^{-1} higher in Gibbs energy, and furthermore they are within a range of less than 3 kcal mol^{-1}. These values do not significantly change when solvent effects are taken into account. Therefore, the main conclusion of this study is that mechanism C, corresponding to addition of the free enol to the aldehyde, is highly favored, at least in the case of reactions catalyzed by iron carbonyl complexes. The Gibbs energies listed in Table 3 are based on geometries and vibrational frequencies obtained with the LANL2DZ basis set. We reoptimized the geometries of **1**, formaldehyde, **5**, **7a**, and the rate-determining transition states at the B3LYP/6-311+G(d,p) level of theory and calculated the corresponding vibrational frequencies. The calculated Gibbs activation energies are very similar to those based on LANL2DZ geometries; the largest difference is 0.4 kcal mol^{-1} for **TS(14-10d)** (Figure 12).

To verify whether the conclusion about the most favorable mechanism holds for other aldehydes, we extended our study to acetaldehyde. We located the rate-determining transitions states for the same reaction paths explored for the reaction with formaldehyde. The structures of these transition states are shown in Figure 13, and the correspond-

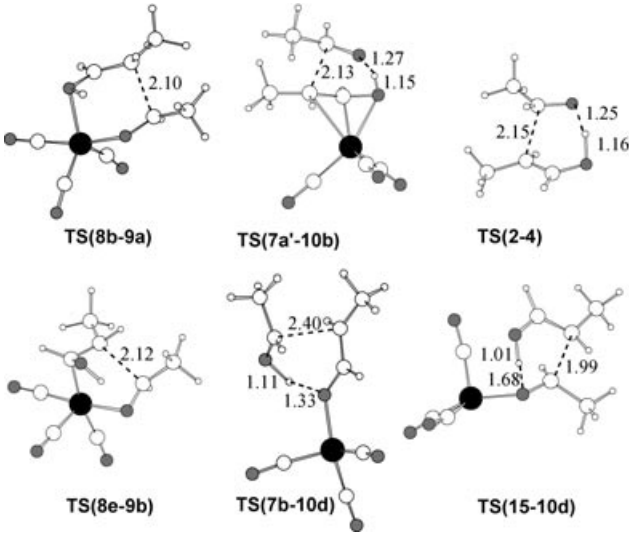

Figure 13. Structures of the rate-determining transition states associated with different paths for the reaction between acetaldehyde and enol **2**. Interatomic distances in Å.

ing Gibbs activation energies are included in Table 3. The presence of the methyl group in the aldehyde increases the Gibbs activation energies by between 2.8 and 7.4 kcal mol^{-1}, depending on the transition state. However, the transition state corresponding to the reaction between free enol and acetaldehyde, **TS(2–4)**, is clearly the most favorable. Hence, the conclusions reached for the reaction of formaldehyde are still valid for acetaldehyde.

Figure 14 schematically presents the catalytic cycle for the tandem reaction involving formation of allylic alcohol and aldol isomerization. The first stage of the process is $Fe(CO)_3$-mediated isomerization of allylic alcohol. The transitions state of highest Gibbs energy corresponds to the enol/allyl alcohol substitution step, which has a Gibbs activation energy of 13.6 kcal mol^{-1} with respect to **5**. After enol decoordination, attack of formaldehyde leads to formation of the aldol **4**. This step involves the transition state with the highest Gibbs energy of the whole process (Gibbs activation energy 15.8 kcal mol^{-1} with respect to the **5**+formaldehyde asymptote). The corresponding Gibbs reaction energy is −15.4 kcal mol^{-1}.

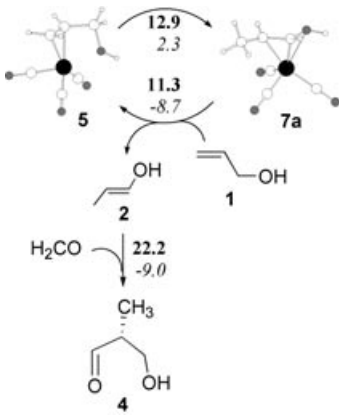

Figure 14. Catalytic cycle for tandem allyl alcohol isomerization/aldol formation. Gibbs activation energies (boldface) and Gibbs reaction energies (italics) in kcal mol^{-1}.

Interestingly, during the Rh^+-mediated isomerization of allyl alcohols to carbonyl compounds, free enols could be characterized by NMR spectroscopy and, in some cases, were even isolated in pure form.[29,30] Furthermore, it has been demonstrated that such enols undergo ene-type addition with very strong electrophiles such as iminium salts, tosyl isocyanate, and tetracyanoethylene.[29b] To the best of our knowledge their possible reactions with aldehydes have been reported only once, as a possible source of byproducts in the isomerization process.[29a]

Starting from the results obtained here it is possible to discuss why the most favorable mechanism for aldol formation involves the reaction between free enol and aldehyde molecules (mechanism C) instead of $Fe(CO)_3$-coordinated species (mechanisms A and B). The formation of the aldol involves two key aspects: the first is an electron transfer from the enol (as a nucleophile) to the electrophilic aldehyde, which is associated with the formation of the new C–C bond, and the second is proton transfer from the enol to the aldehyde. In mechanism C C–C bond formation takes place simultaneously with proton transfer between the enol and the aldehyde, as we observed for the transition state **TS(2–4)** (see Figure 11). An efficient catalyst should be able to favor at least one of these two processes.

Table 4 lists the potential energy barriers associated with the aldol-formation step for the different mechanisms. If we take as the reference the value corresponding to the reaction between free enol and formaldehyde, that is, 9.8 kcal mol^{-1} for **TS(2–4)**, we observe only one case in which the potential energy barrier decreases, namely, **TS(7b-10c)**. For **TS(8b-9a)** and **TS(7a′-10b′)** the barrier increases by less than 4 kcal mol^{-1}, whereas in the remaining two cases, **TS(14–10d)** and **TS(8e-9b)**, the increase is much larger.

Table 4. Potential energy barriers[a] for the aldol-formation step in the different mechanisms.

Mechanism	Transition state[b]	$\Delta E^{\neq}$
A	**TS(8b-9a)**	13.5
A	**TS(8e-9b)**	25.5
B	**TS(7a′-10b′)**	13.6
B	**TS(7b-10c)**	8.9
C	**TS(2-4)**	9.8
C	**TS(14-10d)**	19.5

[a] In kcal mol^{-1}. [b] See Figures 3, 5, 10, 11, and 12.

Mechanism B involves the attack of formaldehyde on a coordinated enol. We considered two different coordination modes: η^3 in **7a**/**7a′**, and η^1 in **7b**. In both complexes the natural population analysis shows that electron charge density is transferred from the enol to the $Fe(CO)_3$ unit (see Table 2), so that the electron-donor ability of the enol molecule decreases and charge transfer from the enol to an incoming aldehyde is not favored. Proton transfer depends on the coordination mode of the enol. For **7a**/**7a′** the Fe–enol interaction involves π orbitals of the ligand. These orbitals do not make any contribution to the O–H bond, so the proton donor ability of the enol is not expected to increase. Thus, the coordinated enol in **7a**/**7a′** is not activated for charge transfer or for proton transfer, and the potential energy for the attack of formaldehyde on **7a′** (13.6 kcal mol^{-1}) is larger than that corresponding to attack on the free enol (9.8 kcal mol^{-1}). On the other hand, when the enol is coordinated in an η^1 mode, as in **7b**, the Fe–enol interaction involves electron donation from an in-plane oxygen sp-type orbital with O–H bonding character (Figure 15). Thus,

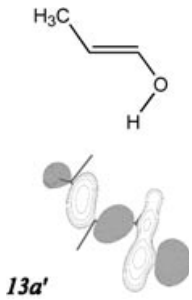

Figure 15. Molecular orbital of **2** involved in the interaction with $Fe(CO)_3$ in **7b**.

coordination to Fe increases the proton donor ability of the enol. For this reason, the potential energy barrier corresponding to attack of formaldehyde on the enol ligand in **7b** (8.9 kcal mol^{-1}) is slightly lower than that corresponding to attack on the free enol, and **TS(7b-10c)** (Figure 10) exhibits a larger degree of proton transfer than **TS(4–2)** (Figure 11). However, **7b** is 9.4 kcal mol^{-1} higher in energy than **7a′**, and therefore **TS(7b-10c)** becomes less favorable than **TS(7a′-10b′)**.

In mechanism A the aldol reaction takes place after coordination of formaldehyde to the [(enol)$Fe(CO)_3$] complex. There are two different modes of coordination: η^1, as in **8b**, and η^2, as in **8e**. The natural population analysis (see Table 1) shows that for **8b** formaldehyde acts as an electron donor, in such a way that it becomes activated for accepting electrons from the enol. However, the enol ligand is not activated, so the potential energy barrier for aldol formation increases with respect to that corresponding to **TS(2–4)**.

On the other hand, for **8e** electron transfer occurs from Fe to formaldehyde, and the aldol-formation step (**8e**→**9b** in Figure 4) involves a much larger potential energy barrier

(25.5 kcal mol^{-1}), since both ligands are electronically deactivated. The same kind of deactivation of the formaldehyde ligand can be observed in **TS(14–10 d)**.

As a consequence of this extensive computational study several important aspects can be emphasized. First, we conclude that the role of the iron tricarbonyl-based catalysts is to favor the allylic alcohol to enol isomerization, which affords the free enol. Then, the aldol product is formed by reaction between the aldehyde and the free enol (mechanism C). The very facile carbonyl-ene-type aldol reaction is noteworthy, since it has not been considered previously in aldol processes and therefore warrants future exploration, both from mechanistic and synthetic point of views. Work along these lines is underway.

Acknowledgement

This work was financially supported by MCyT (BQU2002-0412-C02-01) and DGR (2001SGR-00182). Access to the facilities of the Centre de Supercomputació de Catalunya (CESCA) is gratefully acknowledged. We thank the CNRS and the French Ministry for Education and Research for financial support.

[1] For reviews on the isomerization of allylic alcohols, see a) L. A. Yanovskaya, Kh. Shakhidayatov, *Russ. Chem. Rev.* **1970**, *39*, 859; b) R. C. Van der Drift, E. Bowman, E. Drent, *J. Organomet. Chem.* **2002**, *650*, 1; c) R. Uma, C. Crévisy, R. Grée, *Chem. Rev.* **2003**, *103*, 27.

[2] a) W. A. Herrmann in *Applied Homogeneous Catalysis with Organometallic Compounds*, *Vol. 2* (Eds.: B. Cornils, W. A. Herrmann), VCH, Weinheim, **1996**, p. 980; b) S. G. Davies, *Organotransition Metal Chemistry. Applications to Organic Synthesis*, Pergamon Press, Oxford, **1982**, 266.

[3] a) G. F. Emerson, R. Pettit, *J. Am. Chem. Soc.* **1962**, *84*, 4591; b) R. Damico, T. J. Logan, *J. Org. Chem.* **1967**, *32*, 2356; c) W. T. Hendrix, F. G. Cowherd, J. L. von Rosenberg, *J. Chem. Soc.* **1968**, 97; d) F. G. Cowherd, J. L. von Rosenberg, *J. Am. Chem. Soc.* **1969**, *91*, 2157; e) N. Iranpoor, H. Imanieh, E. J. Forbes, *Synth. Commun.* **1989**, *19*, 2955; f) N. Iranpoor, E. Mottaghinejad, *J. Organomet. Chem.* **1992**, *423*, 399; g) H. Cherkaoui, M. Soufiaoui, R. Grée, *Tetrahedron* **2001**, *57*, 2379.

[4] C. Crévisy, M. Wietrich, V. Le Boulaire, R. Uma, R. Grée, *Tetrahedron Lett.* **2001**, *42*, 395. For a recent application in synthesis, see D. Cuperly, C. Crévisy, R. Grée, *J. Org.* Chem. **2003**, *68*, 6392.

[5] For another recent example, but starting from propargylic alcohols, see: B. M. Trost, S. Oi, *J. Am. Chem. Soc.* **2001**, *123*, 1230.

[6] For a discussion on the atom-economy concept, see: a) B. M. Trost, *Science* **1991**, *254*, 1471; b) B. M. Trost, *Angew. Chem.* **1995**, *187*, 285; *Angew. Chem. Int. Ed. Engl.* **1995**, *34*, 259.

[7] Representative references: a) P. G. Schultz, J. Y. Lin, R. A. Lerner, *Angew. Chem.* **2002**, *114*, 4607; *Angew. Chem. Int. Ed.* **2002**, *41*, 4427; b) B. List, *Tetrahedron* **2002**, *58*, 5573; c) M. Shibasaki, M. Kanai, K. Funabashi, *Chem. Commun.* **2002**, 1989; d) B. M. Trost, E. R. Silcoff, H. Ito, *Org. Lett.* **2001**, *3*, 2497.

[8] R. Uma, N. Gouault, C. Crévisy, R. Grée, *Tetrahedron Lett.* **2003**, *44*, 6187.

[9] R. Uma, M. Davies, C. Crévisy, R. Grée, *Tetrahedron Lett.* **2001**, *42*, 3069.

[10] a) M. Wang, C.-J. Li, *Tetrahedron Lett.* **2002**, *43*, 3589; b) M. Wang, X. -F. Yang, C. -J. Li, *Eur. J. Org. Chem.* **2003**, 998; c) X.-F. Yang, M. Wang, R. S. Varma, C. -J Li, *Org. Lett.* **2003**, *5*, 657.

[11] D. Cuperly, C. Crévisy, R. Grée, *Synlett* **2004**, 93.

[12] V. Branchadell, C. Crevisy, R. Grée, *Chem. Eur. J.* **2003**, *9*, 2062.

[13] a) A. D. Becke, *J. Chem. Phys.* **1993**, *98*, 5648; b) C. Lee, W. Yang, R. G. Parr, *Phys. Rev. B* **1988**, *37*, 785; c) P. J. Stevens, J. F. Devlin, C. F. Chabalowski, M. J. Frisch, *J. Phys. Chem.* **1994**, *98,* 11623.

[14] Gaussian 98, Revision A.9, M. J. Frisch, G. W. Trucks, H. B. Schlegel, G. E. Scuseria, M. A. Robb, J. R. Cheeseman, V. G. Zakrzewski, J. A. Montgomery, Jr., R. E. Stratmann, J. C. Burant, S. Dapprich, J. M. Millam, A. D. Daniels, K. N. Kudin, M. C. Strain, O. Farkas, J. Tomasi, V. Barone, M. Cossi, R. Cammi, B. Mennucci, C. Pomelli, C. Adamo, S. Clifford, J. Ochterski, G. A. Petersson, P. Y. Ayala, Q. Cui, K. Morokuma, D. K. Malick, A. D. Rabuck, K. Raghavachari, J. B. Foresman, J. Cioslowski, J. V. Ortiz, B. B. Stefanov, G. Liu, A. Liashenko, P. Piskorz, I. Komaromi, R. Gomperts, R. L. Martin, D. J. Fox, T. Keith, M. A. Al-Laham, C. Y. Peng, A. Nanayakkara, C. Gonzalez, M. Challacombe, P. M. W. Gill, B. Johnson, W. Chen, M. W. Wong, J. L. Andres, C. Gonzalez, M. Head-Gordon, E. S. Replogle, J. A. Pople, Gaussian, Inc., Pittsburgh, PA, **1998**.

[15] C. Peng, P. Y. Ayala, H. B. Schlegel, M. J. Frisch, *J. Comput. Chem.* **1996**, *17*, 49.

[16] a) C. Gonzalez, H. B. Schlegel, *J. Chem. Phys.* **1989**, *90*, 2154; b) C. Gonzalez, H. B. Schlegel, *J. Phys. Chem.* **1990**, *94*, 5523.

[17] a) T. H. Dunning, Jr., P. J. Hay In *Modern Theoretical Chemistry*, *Vol. 3* (Ed: H. F. Schaefer III), Plenum, New York, **1976**, p. 1; b) P. J. Hay, W. R. Wadt, *J. Chem. Phys.* **1985**, *82*, 299.

[18] A. E. Reed, L. A. Curtiss, F. Weinhold, *Chem. Rev.* **1988**, *88*, 899.

[19] a) A. Klamt, G. Schürmann, *J. Chem. Soc. Perkin Trans. 2* **1993**, 799; b) V. Barone, M. Cossi, *J. Phys. Chem. A* **1998**, *102*, 1995.

[20] a) R. Krishnan, J. S. Binkley, R. Seeger, J. A. Pople, *J. Chem. Phys.* **1980**, *72*, 650; b) A. J. H. Wachters, *J. Chem. Phys.* **1970**, *52*, 1033; c) P. J. Hay, *J. Chem. Phys.* **1977**, *66*, 4377.

[21] Y. Zhao, B. J. Lynch, D. G. Truhlar, *J. Phys. Chem. A* **2004**, *108*, 2715.

[22] A. D. Becke, *Phys. Rev. A* **1988**, *38*, 3098.

[23] A. D. Becke, *J. Chem. Phys.* **1996**, *104*, 1040.

[24] Gaussian 03, Revision B.04, M. J. Frisch, G. W. Trucks, H. B. Schlegel, G. E. Scuseria, M. A. Robb, J. R. Cheeseman, J. A. Montgomery, Jr., T. Vreven, K. N. Kudin, J. C. Burant, J. M. Millam, S. S. Iyengar, J. Tomasi, V. Barone, B. Mennucci, M. Cossi, G. Scalmani, N. Rega, G. A. Petersson, H. Nakatsuji, M. Hada, M. Ehara, K. Toyota, R. Fukuda, J. Hasegawa, M. Ishida, T. Nakajima, Y. Honda, O. Kitao, H. Nakai, M. Klene, X. Li, J. E. Knox, H. P. Hratchian, J. B. Cross, C. Adamo, J. Jaramillo, R. Gomperts, R. E. Stratmann, O. Yazyev, A. J. Austin, R. Cammi, C. Pomelli, J. W. Ochterski, P. Y. Ayala, K. Morokuma, G. A. Voth, P. Salvador, J. J. Dannenberg, V. G. Zakrzewski, S. Dapprich, A. D. Daniels, M. C. Strain, O. Farkas, D. K. Malick, A. D. Rabuck, K. Raghavachari, J. B. Foresman, J. V. Ortiz, Q. Cui, A. G. Baboul, S. Clifford, J. Cioslowski, B. B. Stefanov, G. Liu, A. Liashenko, P. Piskorz, I. Komaromi, R. L. Martin, D. J. Fox, T. Keith, M. A. Al-Laham, C. Y. Peng, A. Nanayakkara, M. Challacombe, P. M. W. Gill, B. Johnson, W. Chen, M. W. Wong, C. Gonzalez, J. A. Pople, Gaussian, Inc., Pittsburgh, PA, **2003**.

[25] K. Raghavachari, G. W. Trucks, J. A. Pople, M. Head-Gordon, *Chem. Phys. Lett.* **1989**, *157*, 479.

[26] a) R. S. Berry, *J. Chem. Phys.* **1960**, *32*, 933; b) R. S. Berry, *Rev. Mod. Phys.* **1960**, *32*, 447; c) D. R. Eaton, *J. Am. Chem. Soc.* **1968**, *90*, 4272. d) A. R. Rossi, R. Hoffmann, *Inorg. Chem.* **1974**, *13*, 365.

[27] To obtain the same stereostructure as in mechanism A for aldol **4** we started from **7a′** instead of its enantiomer **7a**.

[28] E. L. Coitiño, J. Tomasi, O. N. Ventura, *J. Chem. Soc. Faraday Trans.* **1994**, *90*, 1745.

[29] a) C. S. Chin, S. Y. Lee, J. Park, S. Kim, *J. Am. Chem. Soc.* **1988**, *110*, 8244; b) S. H. Bergens, B. Bosnich, *J. Am. Chem. Soc.* **1991**, *113*, 958.

[30] For some other leading references on free enols, see a) H. Hart, *Chem. Rev.* **1979**, *79*, 515; b) J. -L. Rippoll, *Nouv. J. Chim.* **1979**, *3*, 195; c) H. Hart, M. J. Sasaoka, *J. Chem. Educ.* **1980**, *57*, 685; d) B. Capon, D. S. Rycroft, T. W. Watson, C. Zucco, *J. Am. Chem. Soc.* **1981**, *103*, 1761; e) Z. Rappoport, S. E. Biali, *Acc. Chem. Res.* **1988**, *21*, 442.

Received: May 12, 2004
Published online: October 7, 2004

